SUPPLEMENTARY INFORMATION

Non-invasive *in vivo* imaging of tumour-associated cathepsin B by a highly selective inhibitory DARPin

Lovro Kramer[1,2], Miha Renko[1], Janja Završnik[1,2], Dušan Turk[1,3], Markus A. Seeger[4], Olga Vasiljeva[1], Markus G. Grütter[5], Vito Turk[1], Boris Turk[1,3]*

[1] Jozef Stefan Institute, Department of Biochemistry and Molecular and Structural Biology, Ljubljana (Slovenia)

[2] International Postgraduate School Jozef Stefan, Ljubljana (Slovenia)

[3] Center of Excellence CIPKEBIP, Ljubljana (Slovenia)

[4] Institute of Medical Microbiology, University of Zürich, Zürich (Switzerland)

[5] Department of Biochemistry, University of Zürich, Zürich (Switzerland)

*correspondence: boris.turk@ijs.si

SUPPLEMENTARY METHODS

Expression and purification of recombinant cathepsins

Human and mouse cathepsin B (CatB) were expressed in inclusion bodies of *Escherichia coli* and purified as described previously in [1] and [2], respectively. Other cathepsins were expressed in *Pichia pastoris* and purified as described previously for cathepsins L and S [3], cathepsin K [4] and cathepsin X [5].

Biotinylation of human CatB, mouse CatB and human CatS

Recombinant human CatB, mouse CatB and human CatS were biotinylated with EZ-Link™ Sulfo-NHS-LC-LC-Biotin (Thermo Fisher Scientific) in PBS (pH 7.0) at 4°C for 2 h. The residual reagent was removed by gel filtration on PD10 columns (GE Healthcare Life Sciences), and the biotinylation efficiency was confirmed by Western blot and mass spectrometry (Fig. S16).

Ribosome display selection of cathepsin B-specific inhibitory DARPins

The aim of the study was to obtain DARPins that bind both human and mouse cathepsin B with high selectivity and affinity. We performed ribosome display of the recently described DARPin 2.0 library [6] against both CatB orthologues. Ribosome display was performed as described [6, 7], with some modifications. After four rounds of selection against human CatB, four subsequent rounds of selection against mouse CatB were performed. Each selection round included a prepanning step with biotinylated MBP and all rounds were carried out with the surface panning method using NeutrAvidin coated immunotubes (first and fifth round) or 96-well plates (all other rounds). The washing times in the ribosome display were 3 × 10 s in the first and fifth round, 3 × 10 min in the second and sixth round, 3 × 15 min in the third and seventh round and 3 × 30 min in the fourth and eighth round. Retrieved DNA from the last round was cloned into pBXNH3 [8] and transformed into E. coli MC1061, and single colonies were grown. Approximately 1000 colonies were inoculated in Terrific Broth and grown in 96-

well deep well plates until OD(600) = 0.5, and DARPin expression was induced by 0.01% L-arabinose and carried out for 24 h at 37°C. Crude cell extracts were obtained as described [6] and used in ELISA screening.

Crude cell ELISA screening

Biotinylated cathepsins were immobilized onto NeutrAvidin-coated 384-well plates and crude E. coli extracts with expressed DARPins were incubated as described previously [6]. Any bound and unwashed DARPins were detected with HRP-conjugated anti-His antibody (Roche) used for colorimetric detection. Forty unique clones that produced the highest signal for human and mouse cathepsin B and lacked signal for the highly homologous cathepsin S were chosen for further analysis.

Large scale DARPin production

Forty DARPin clones from the selection process were cloned into the pQE30 vector (Qiagen) with the primers 5'-CGCGGATCCGACCTGGGTAAGAA-3' and 5'-GCATAATTAAGCTTTGCCGCTTTTTGC-3' and transformed into *E. coli* XL-1 Blue cells. Expression was performed using auto-inducing medium [9]. Purification included standard Ni^{2+} affinity chromatography (wash and elution buffer were 50 mM Tris/HCl, pH 7.4, 500 mM NaCl, 10% glycerol and 20 mM or 250 mM imidazole, respectively). These DARPins were subjected to binding and inhibition assays. DARPins *8h6* and *81* displayed exceptionally strong binding and were therefore selected for further characterization. As a negative control, a nonspecific DARPin *E3_5* [10] was used throughout the experiments.

DARPins *81*, *8h6* and *E3_5*, which were used in subsequent experiments, were further purified by size-exclusion chromatography (SEC) on Superdex S-200 (GE Healthcare) in 20 mM sodium phosphate, pH 7.0, 150 mM NaCl. In the case of purification for SPR experiments, 0.005% Tween-20 was added. When DARPins were used in experiments with cell cultures or mice, a washing step including Triton X-114 was added to the Ni^{2+} affinity chromatography as described [11].

C-terminal site-specific labelling of DARPins

In order to achieve site-specific labelling, a C-terminal cysteine was introduced into the DARPin sequences via PCR using the primers 5'-CGCGGATCCGACCTGGGTAAGAA-3' and 5'-CCCAAGCTTTTATTAACAGGACCCCGCCGCTTTTTGC-3' and subsequent cloning into pQE30 via *Bam*HI and *Hin*dIII. The DARPins were expressed and purified as described above.

DARPins were labelled with EZ-Link™ Maleimide-PEG2-Biotin (Thermo Fisher Scientific) or Cyanine5.5 (Cy5.5) maleimide (Lumiprobe) according to manufacturers' recommendations. Briefly, DARPins were reduced with 50 mM TCEP for 30 min at room temperature. TCEP was removed by SEC using PD-10 columns equilibrated with 20 mM sodium phosphate, pH 7.0, 150 mM NaCl. Reduced DARPins (500 μM) were labelled for 1.5 hour at room temperature with the addition of 20-time and 2-time molar access of EZ-Link™ Maleimide-PEG2-Biotin and Cy5.5 maleimide, respectively. The reaction and subsequent steps were performed in the dark in the case of Cy5.5 labelling. Residual reagents were removed by SEC using PD-10 columns and concentrated using Amicon Ultra-4 Centrifugal Filter Units with a 10-kDa cut-off (EMD Millipore). Due to small residual amounts of unlabelled DARPins in the case of Cy5.5 labelling, an additional purification step using a MonoQ 5/50 anion exchange column (GE Healthcare) was used with a linear gradient from 10-1000 mM NaCl in 100 mM sodium bicarbonate, pH 8.0. Monolabelled DARPins were separated from unlabelled DARPins based on the additional charge of dye.

To determine the efficiency of DARPin labelling with biotin, proteins were separated via SDS-PAGE and blotted, and detection with streptavidin-HRP was performed (Fig. S2).

To determine whether DARPins were efficiently labelled with Cy5.5, they were separated on SDS-PAGE and Cyanine5.5 fluorescence was measured using a fluorescent imager (Typhoon, GE Healthcare). Silver staining was performed to confirm the amount of loaded protein (Fig. S3).

SUPPLEMENTARY FIGURES

a

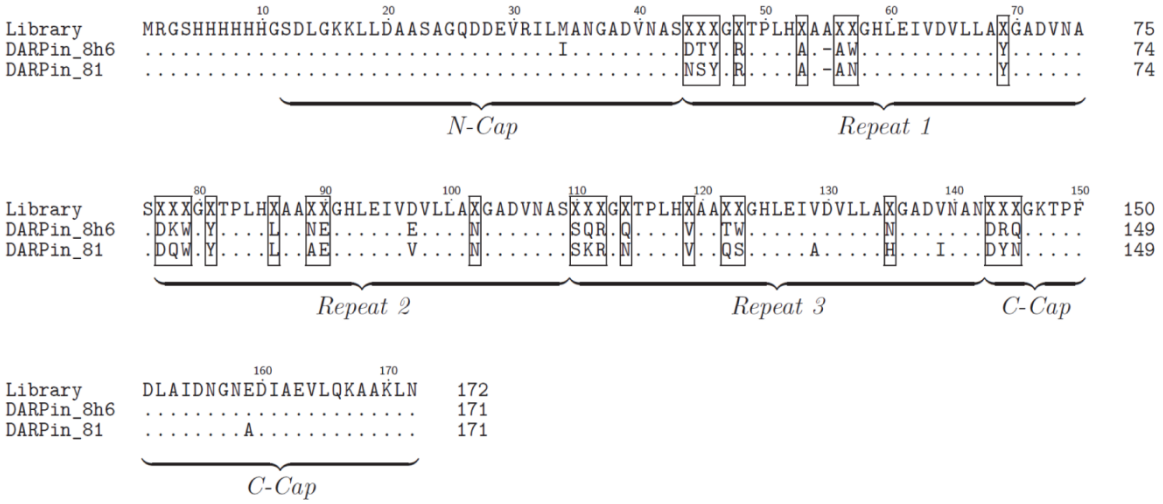

b

DARPin E3_5
MRGSHHHHHHGSDLGKKLLEAARAGQDDEVRILMANGADVNATDNDGYTPLHLAASNGHLEIVEVLLKNGADVNASDLTGITPLHLAAATGHLEIVEVL
LKHGADVNAYDNDGHTPLHLAAKYGHLEIVEVLLKHGADVNAQDKFGKTAFDISIDNGNEDLAEILQKLN

DARPin E3_5_GSC
MRGSHHHHHHGSDLGKKLLEAARAGQDDEVRILMANGADVNATDNDGYTPLHLAASNGHLEIVEVLLKNGADVNASDLTGITPLHLAAATGHLEIVEVL
LKHGADVNAYDNDGHTPLHLAAKYGHLEIVEVLLKHGADVNAQDKFGKTAFDISIDNGNEDLAEILQGSC

DARPin 8h6_GSC
MRGSHHHHHHGSDLGKKLLDAASAGQDDEVRILIANGADVNASDTYGRTPLHAAAWGHLEIVDVLLAYGADVNASDKWGYTPLHLAANEGHLEIVEVLL
ANGADVNASSQRGQTPLHVAATWGHLEIVDVLLANGADVNANDRQGKTPFDLAIDNGNEDIAEVLQKAAGSC

DARPin 81_GSC
MRGSHHHHHHGSDLGKKLLDAASAGQDDEVRILMANGADVNASNSYGRTPLHAAANGHLEIVDVLLAYGADVNASDQWGYTPLHLAAAEGHLEIVVVLL
ANGADVNASSKRGNTPLHVAAQSGHLEIADVLLAHGADINANDYNGKTPFDLAIDNGNADIAEVLQKAAGSC

Figure S1 | DARPins sequences. (a) Sequences of DARPins *8h6* and *81*, selective binders of CatB. The sequences are aligned with the DARPin 2.0 library [6], the source of these DARPins. **(b)** Sequences of the non-selective (naïve) DARPin *E3_5* [12] and the C-terminal mutants of DARPins *E3_5*, *8h6* and *81*, that were used for biotin or Cy5.5 labelling.

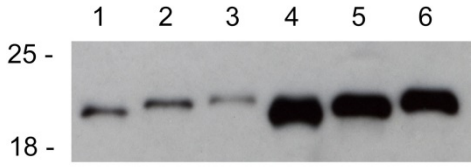

Figure S2 | Biotinylation efficiency of DARPins. Labelled DARPins were separated via SDS-PAGE, and Western blotting was performed. Detection of the biotin tag was performed using streptavidin-HRP. 1 = 3.6 ng DARPin *E3_5*-biotin, 2 = 3.6 ng DARPin *81*-biotin, 3 = 3.6 ng DARPin *8h6*-biotin, 4 = 36 ng DARPin *E3_5*-biotin, 5 = 36 ng DARPin *81*-biotin, 6 = 36 ng DARPin *8h6*-biotin

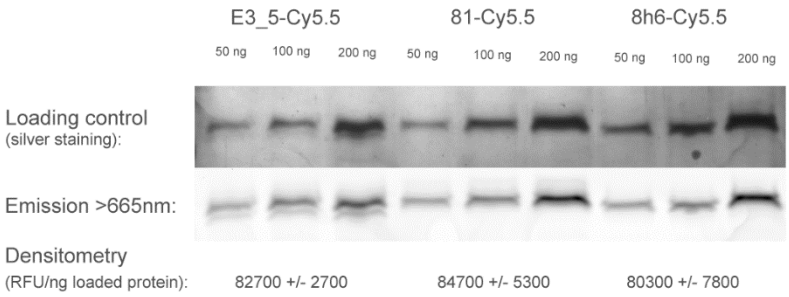

Figure S3 | Cy5.5 labelling of DARPins. Labelled DARPins (50 μg, 100 μg or 200 μg of each) were separated via SDS-PAGE, and Cy5.5 fluorescence was detected using a fluorescence scanner (Typhoon). Densitometry revealed no significant differences in the labelling efficiency, confirming successful site-specific labelling of the C-terminal cysteine. To confirm the amounts of loaded DARPins, silver staining of the gels was performed.

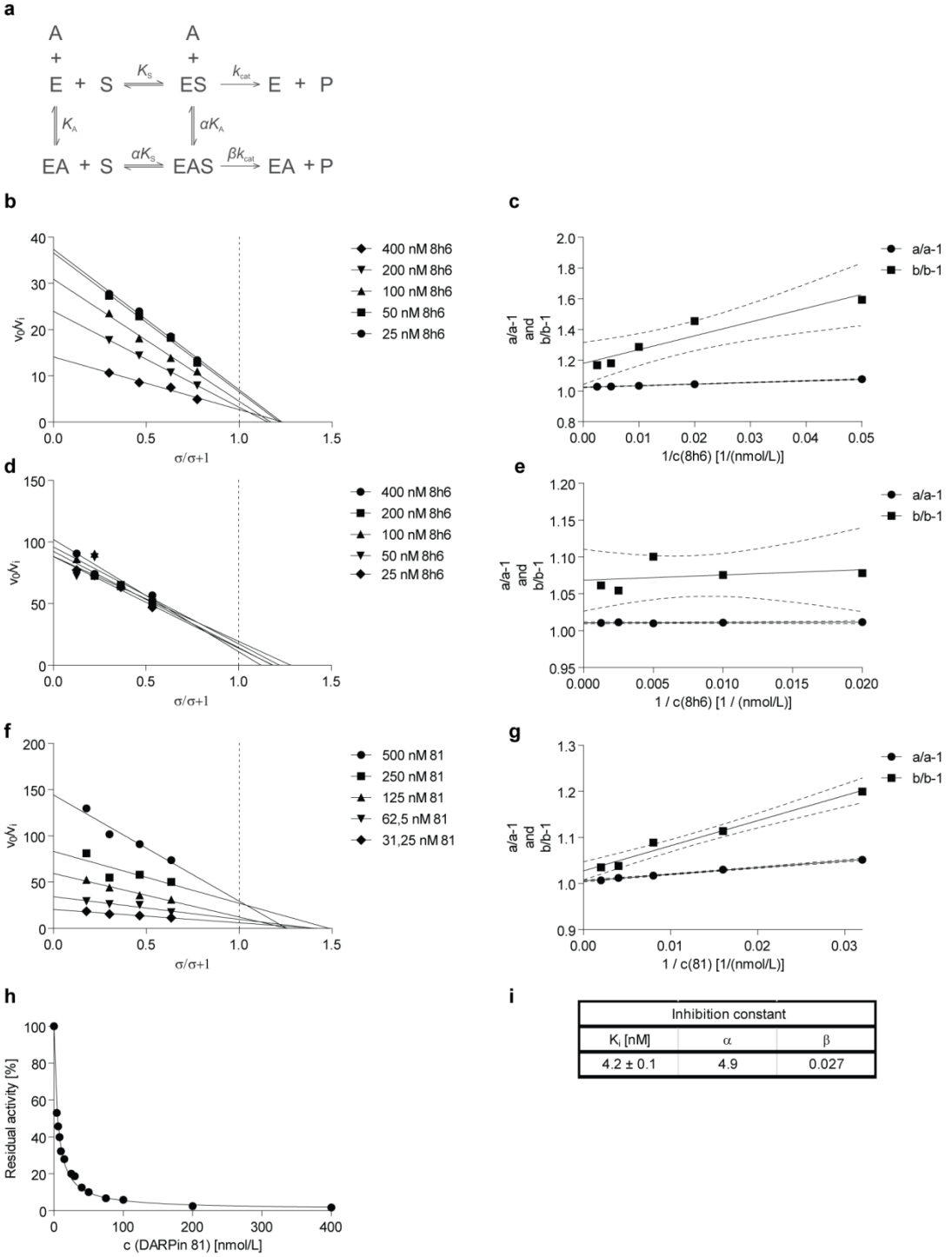

Figure S4 | Characterization of CatB inhibition by DARPins *8h6* and *81*. (**a**) The general modifier scheme depicting the kinetic parameters α and β. E, enzyme; A, inhibitor; S, substrate; P, product. (**b**) Primary specific velocity plot using 1 nM hCatB, increasing concentrations of substrate z-Arg-Arg-AMC (K_M = 173 μM) and increasing concentrations of

DARPin *8h6*. The intersections of the linear regression fits are on the right side of $\sigma/(\sigma+1) = 1$, which is characteristic of mixed type inhibition, with contributing competitive and uncompetitive modes; σ = [substrate]/K_M. (**c**) Secondary specific velocity plot, replotted from **b**. The parameters α correspond to the v_0/v_i values of the linear fits in plot **b** at $\sigma/(\sigma+1) = 0$, the parameters β correspond to the v_0/v_i values of the linear fits in plot **b** at $\sigma/(\sigma+1) = 1$. Linear least squares fits are shown in solid lines. The analysis yielded the mechanistic parameters $\alpha = 6.6$ and $\beta = 0.15$, corresponding to hyperbolic mixed-mode inhibition. (**d**) Primary specific velocity plot using 1 nM mCatB, increasing concentrations of substrate z-Arg-Arg-AMC (K_M = 262 μM) and increasing concentrations of DARPin *8h6*. The intersections of the linear regression fits are on the right side of $\sigma/(\sigma+1) = 1$, which is characteristic for mixed inhibition, with contributing competitive and uncompetitive modes. (**e**) Secondary specific velocity plot, replotted from **d**. The analysis yielded the mechanistic parameters $\alpha = 6.1$ and $\beta = 0.064$, corresponding to hyperbolic mixed mode inhibition. (**f**) Primary specific velocity plot using 1 nM hCatB, increasing concentrations of substrate z-Arg-Arg-AMC (K_M = 173 μM) and increasing concentrations of DARPin *81*. The intersections of the linear regression fits are on the right side of $\sigma/(\sigma+1) = 1$, which is characteristic of mixed type of inhibition, with contributing competitive and uncompetitive modes. (**g**) Secondary specific velocity plot, replotted from **f**. The analysis yielded the mechanistic parameters α = 4.9 and $\beta = 0.027$, corresponding to hyperbolic mixed mode inhibition. (**h**) Inhibition of hCatB with DARPin *81.* The solid line shows the non-linear least squares fit of residual enzyme activity (% of uninhibited) for tight-binding conditions, as described in [13]. (**i**) Collected results of the kinetic characterization of binding of DARPin *81* to hCatB.

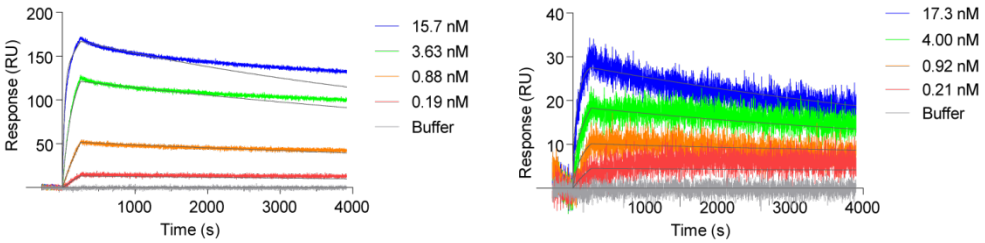

Figure S5 | Kinetics of DARPin 8h6 binding to human and mouse CatB determined by surface plasmon resonance. Biotinylated human CatB (left) and mouse CatB (right) were immobilized on a NeutrAvidin-coated NLC chip using ProteOn XPR36. Increasing concentrations of DARPin *8h6* were then flowed through the chip, and the response was monitored. The sensograms were fitted in ProteOn Manager Software (version 3.1.0.6, Bio-Rad Laboratories) using the heterogeneous ligand model fit [14]. The kinetic parameters are represented in Table 1.

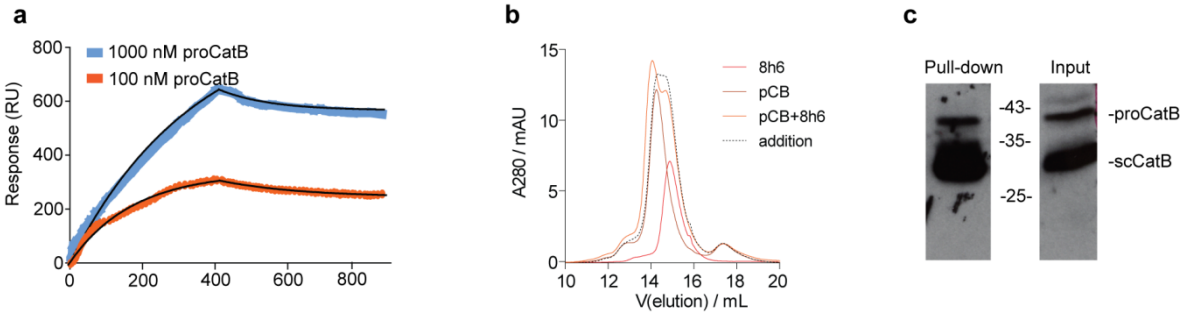

Figure S6 | DARPin *8h6* interacts with the zymogen form of cathepsin B (proCatB). (**a**) SPR measurements. Biotinylated DARPin *8h6* was immobilized on a NeutrAvidin-coated NLC chip using BiaCore X. Two concentrations of human proCatB were then flowed through the chip, and the response was monitored. The sensograms were fitted in Prism (GraphPad). The kinetic parameters are represented in Table 1 in the main text. (**b**) Size-exclusion chromatography of procathepsin B C29S in complex with DARPin *8h6.* First, procathepsin B C29S (brown) and DARPin *8h6* (red) were run separately using Superdex S200 size exclusion chromatography. The mixture (molar ratio DARPin *8h6*:proCatB = 2:1) of the proteins was incubated for 10 minutes and run on the size exclusion column (orange). There is a leftward shift compared to the theoretical addition of elution spectra (dotted) that corresponds to the formation of the complex. (**c**) Western blot analysis of streptavidin pull-down from THP-1 cell lysate incubated with C-terminally biotinylated DARPin *8h6*. The streptavidin-bound fraction was separated on SDS-PAGE and immunoblotted against CatB. Total cell lysate (input) was added to visualize different forms of CatB present.

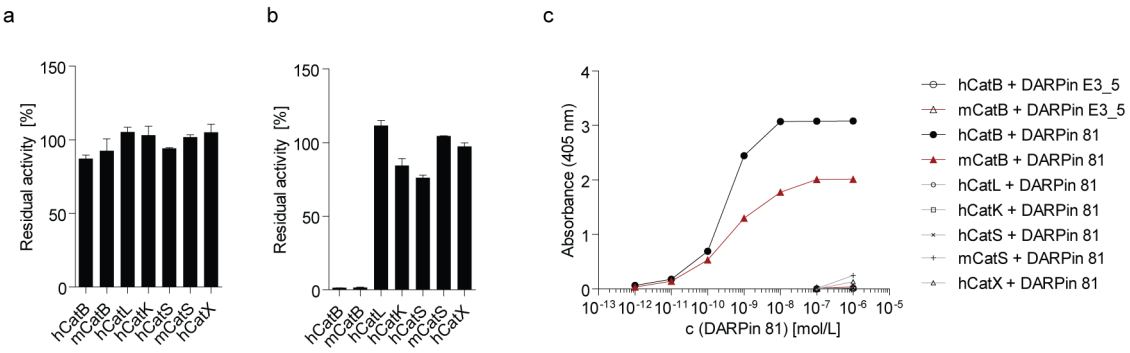

Figure S7 | Effect of DARPins *E3_5* and *81* on cathepsin activity and binding. (**a**) Residual proteolytic activity (% of uninhibited) of recombinant cathepsins (human CatB 1 nM, mouse CatB 1 nM, human CatL 1 nM, human CatK 1 nM, human CatS 10 nM, mouse CatS 10 nM, human CatX 250 nM) in the presence of 10 μM nonselective DARPin *E3_5* (**b**) or CatB-selective DARPin *81*; z-Arg-Arg-AMC was used for measuring CatB activity and z-Phe-Arg-AMC for other cathepsins. The experiment was performed in triplicate and is presented as the mean ± standard error. (**c**) Colorimetric affinity assay with immobilized recombinant cathepsins (50 nM). Increasing concentrations of C-terminally biotinylated DARPin *81* or *E3_5* were incubated in 96-well plates with immobilized recombinant cathepsins. After washing, the biotin tag was detected by streptavidin-HRP.

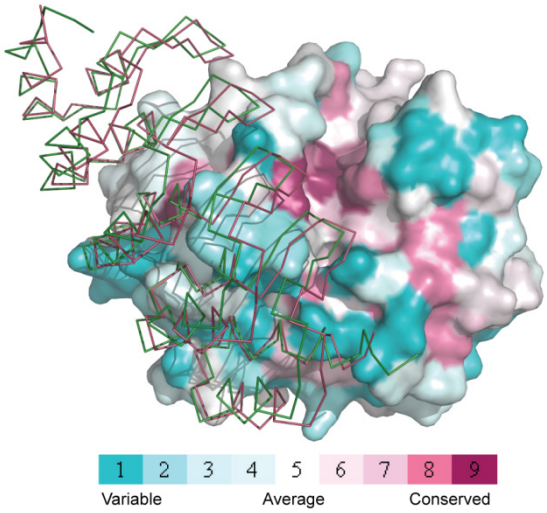

Figure S8 | Amino acid conservation within the cathepsin family in CatB. Sequences of mature human cysteine cathepsins were aligned using Clustal Omega (http://www.ebi.ac.uk/Tools/msa/clustalo/), and amino acid conservation (similarity) was determined by ConSurf (http://consurf.tau.ac.il/) using the Bayesian method. The conservation is shown as a colour-map on the three-dimensional structure of CatB from the CatB-DARPin *81* complex. DARPin *8h6* is from the crystal structure of CatB-DARPin *8h6* complex and is superimposed. The image was produced in PyMOL (www.pymol.org).

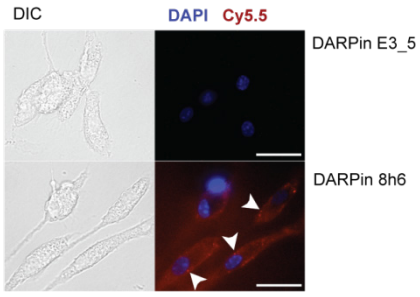

Figure S9 | DARPin *8h6* cell surface association imaged by fluorescence microscopy. Active endocytosis of dBMMs grown on glass coverslips was blocked by 30 min incubation on 4°C followed by incubation with 100 nM Cy5.5-labelled DARPin *8h6* or DARPin *E3_5* at 4°C for 15 min (red). Cell nuclei were stained with DAPI (blue) followed by immediate microscope imaging. Differential interference contrast (DIC) images were collected for visualization of whole cells. White arrows point to sites of DARPin *8h6* binding to membrane-associated CatB.

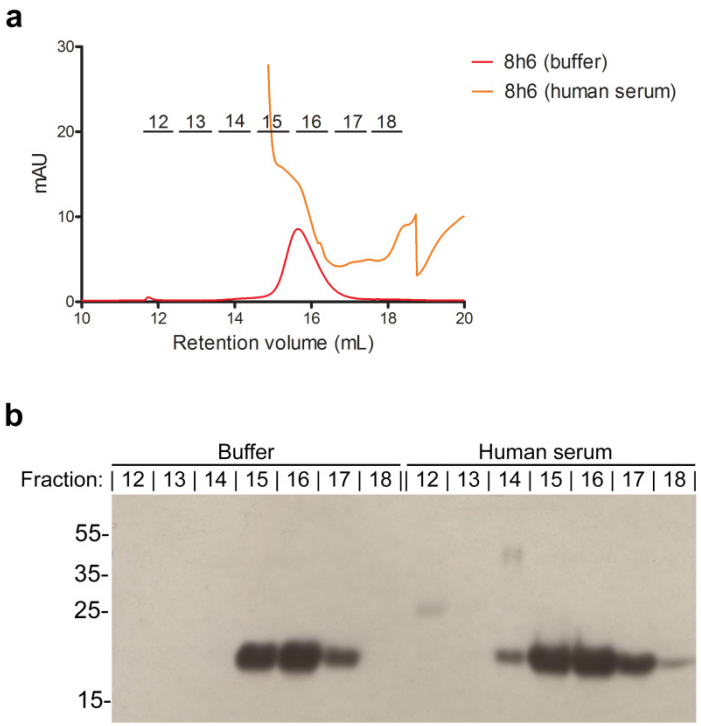

Figure S10 | Serum stability of DARPin *8h6*. (**a**) Biotinylated DARPin *8h6* was incubated in human serum for 24 h at 37°C, followed by separation using size-exclusion chromatography (orange line). As a control, the same concentration of biotinylated DARPin 8h6 without human serum was used (red line). (**b**) Proteins from collected fractions (F12-F18) were separated using SDS-PAGE and Western blotting was performed. The biotin tag was detected by streptavidin-HRP. DARPin *8h6* was present in the same fractions in both samples, with minimal peak broadening in the serum sample.

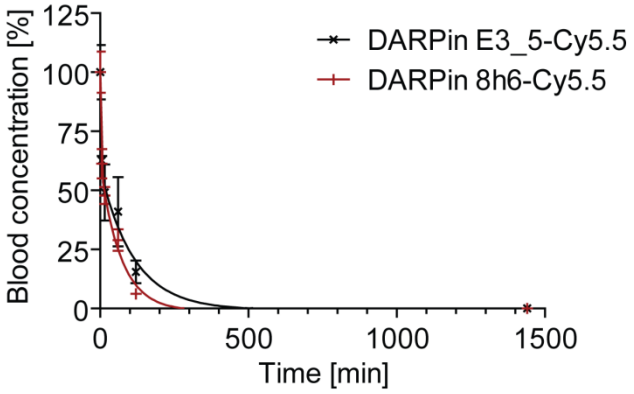

	Half Life (Fast) [min]
DARPin E3_5-Cy5.5	1.8
DARPin 8h6-Cy5.5	1.6

	Half Life (Slow) [min]
DARPin E3_5-Cy5.5	78.8
DARPin 8h6-Cy5.5	48.5

Figure S11 | Blood clearance of Cy5.5-labelled DARPins *E3_5* and *8h6*. DARPins (1 nmol) were administered intravenously and blood samples were collected after 0 min, 5 min, 15 min, 60 min, 120 min and 1440 min. The concentration of the DARPin in the blood was determined by measuring Cy5.5 fluorescence (ex/em = 670/710 nm) using a Tecan Infinite plate reader and comparing the signals to a standard curve.

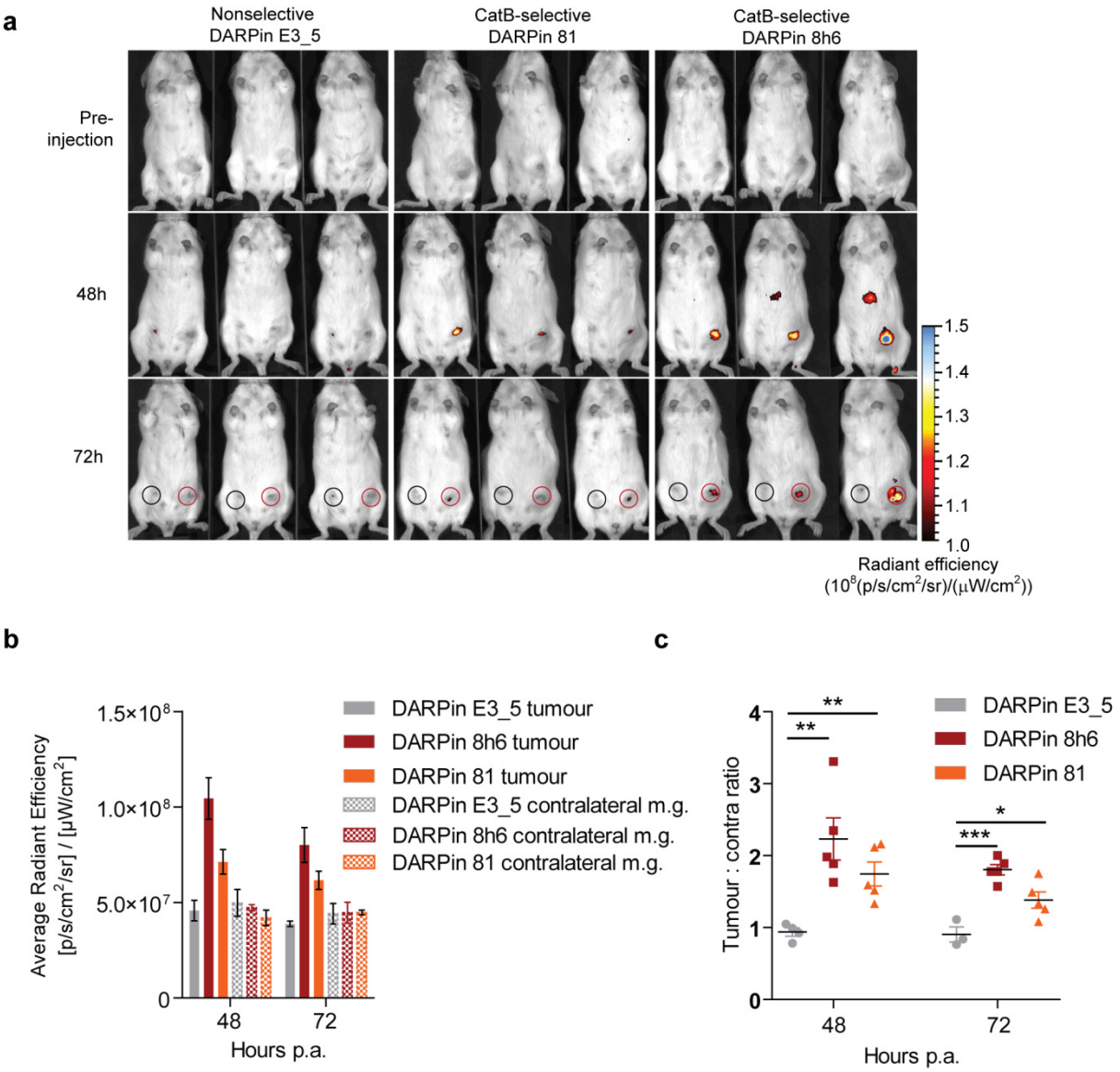

Figure S12 | Non-invasive optical tumour imaging using fluorescently labelled DARPins *E3_5*, *81* and *8h6* at late time-points (48 h, 72 h) in PyMT tumour model. (**a**) Mice from the experiments in Fig. 5 and Fig. S14 were additionally imaged after 48 h and 72 h in the same way as described in Fig. 5. As controls, the images of mice before any DARPin administration (pre-injection) are also shown. Note the different fluorescent scale used in this image and in Fig. 5 and Fig. S14 (**b**) Quantification of average radiant efficiency from **a** in tumours and contralateral mammary glands as the means ± standard error. The regions of interest (ROI): tumour – red circle; contralateral mammary gland – black circle. (**c**) Tumour-

to-contralateral mammary gland ratios of average radiant efficiency in individual mice from **a** represented as the means ± standard error.

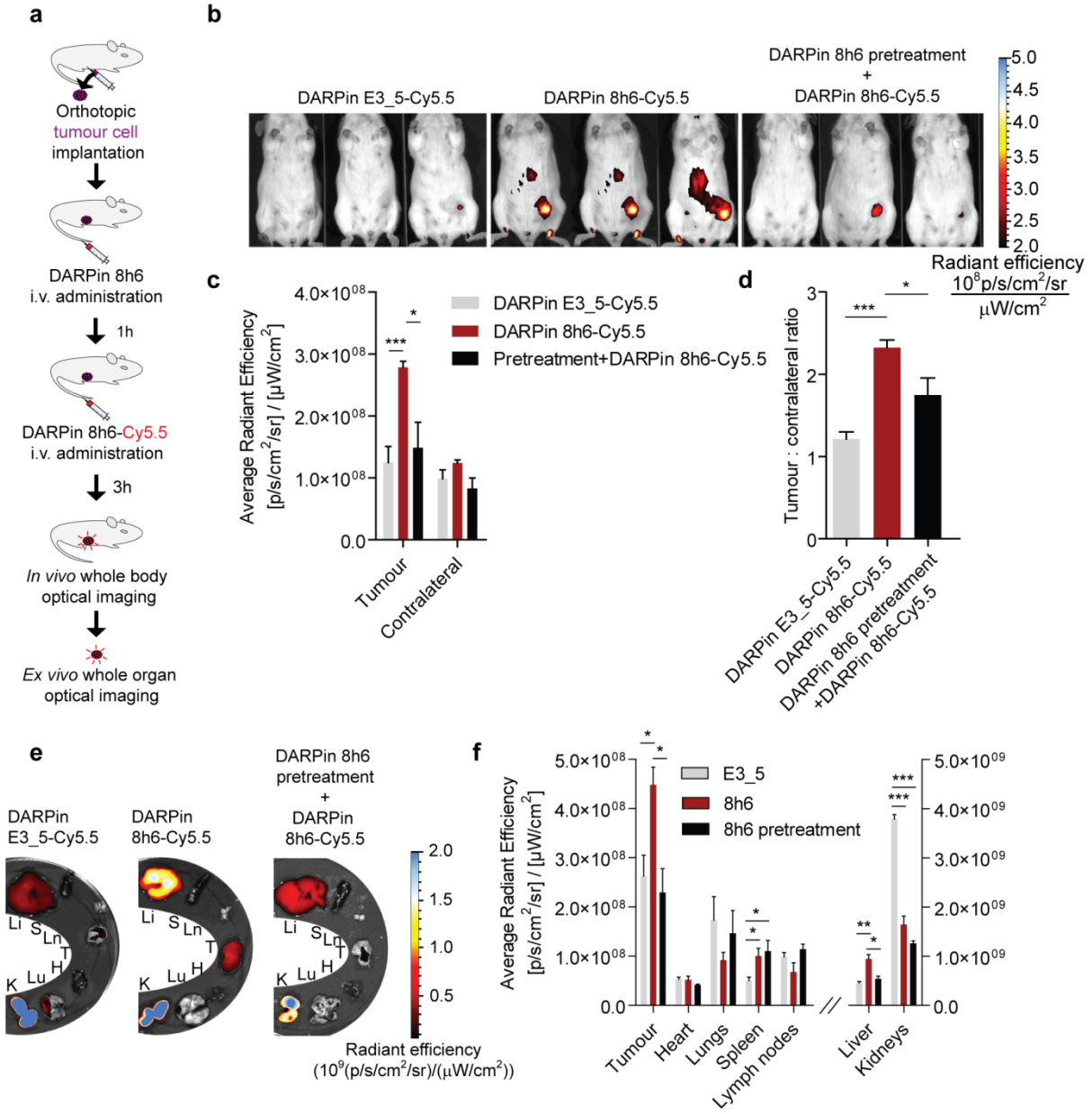

Figure S13 | *In vivo* competition assay with unlabelled DARPin *8h6* in the PyMT model.

(**a**) Schematic representation of the *in vivo* competition experiment outline (**b**) PyMT cells were injected into the left inguinal fat pads of FVB/N mice and allowed to grow until 100-150 mm^3. Unlabelled DARPin *8h6* was injected intravenously (10 nmol in 100 µL). After 1 h, Cy5.5-labelled DARPin *8h6* was injected intravenously (1 nmol in 100 µL) and epi-fluorescent images were taken 3 h later. False blue-hot colouring of the radiant efficiency (radiance (photons per second per square centimetre per steradian) per incident excitation power (microwatt per square cm)) is overlaid on bright-field images. The DARPin E3_5-Cy5.5 and DARPin 8h6-Cy5.5 groups from Fig. 5b are shown for comparison (**c**)

Quantification of the average radiant efficiency from **b** in tumours and contralateral mammary glands as the means ± standard error. Regions of interest (ROI) were chosen in the same way as in Fig. 5. The DARPin E3_5-Cy5.5 and DARPin 8h6-Cy5.5 groups from Fig. 5c are shown for comparison (**d**) Tumour-to-contralateral mammary gland ratios of the average radiant efficiency in individual mice from **b** represented as the means ± standard error. The DARPin E3_5-Cy5.5 and DARPin 8h6-Cy5.5 groups from Fig. 5b are shown for comparison (**e**) DARPin distribution in isolated organs 3 h after administration of Cy5.5 labelled DARPin *8h6*. False blue-hot images of the radiance efficiency are overlaid on bright-field images. Representative images of four mice per group are shown. The DARPin E3_5-Cy5.5 and DARPin 8h6-Cy5.5 groups from Fig. 5b are shown for comparison Li = liver, S = spleen, Ln = lymph nodes, T = tumour, H = heart, Lu = lungs, K = kidneys. (**f**) The average radiant efficiency from isolated organs is quantified as the mean ± standard error. The DARPin E3_5-Cy5.5 and DARPin 8h6-Cy5.5 groups from Fig. 5b are shown for comparison *** $p<0.001$, ** $p<0.01$, * $p<0.05$

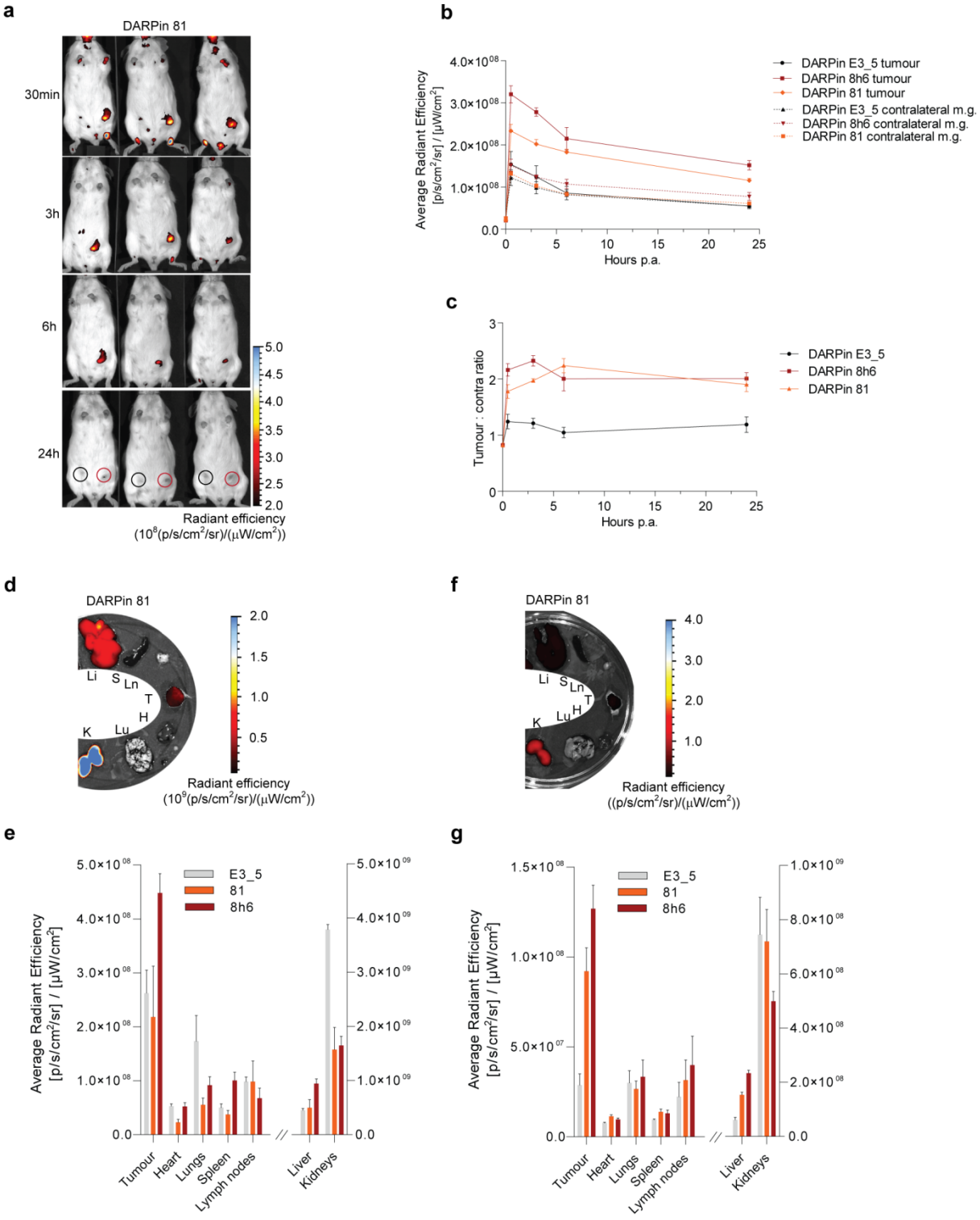

Figure S14 | Non-invasive optical tumour imaging by fluorescently labelled DARPin *81* in PyMT tumour model and comparison with DARPins *E3_5* and *8h6* (**a**) PyMT cells were injected into the left inguinal fat pads fat pads of FVB/N mice and allowed to grow to 100-150 mm^3. C-terminally Cy5.5-labelled DARPin *81* was injected intravenously (1 nmol in

100 μL) and epi-fluorescent images were taken at designated time-points after administration. False blue-hot colouring of radiant efficiency (radiance (photons per second per square centimetre per steradian) per incident excitation power (microwatt per square cm)) is overlaid on bright-field images. (**b**) Quantification of average radiant efficiency from **a** in tumours and contralateral mammary glands as the means ± standard error. The regions of interest (ROI): tumour – red circle; contralateral mammary gland – black circle. For comparison the data for DARPins *8h6* and the nonselective DARPin *E3_5* from the article main text Fig. 5c were added. (**c**) Tumour-to-contralateral mammary gland ratios of average radiant efficiency in individual mice from **a** represented as the means ± standard error. For comparison the data for DARPins *8h6* and the nonselective DARPin *E3_5* from the article main text Fig. 5d were added. (**d, e**) Imaging and quantification of DARPin distribution in isolated organs 3 h and (**f, g**) 72 h after administration. False blue-hot images of radiance efficiency are overlaid on bright-field images. Representative images (three per group) are shown. The average radiant efficiency from each organ is quantified bellow as the mean ± standard error and the data for DARPins *8h6* and *E3_5* from the article main text Figs. 5g, h were added for comparison. Li = liver, S = spleen, Ln = lymph nodes, T = tumour, H = heart, Lu = lungs, K = kidneys

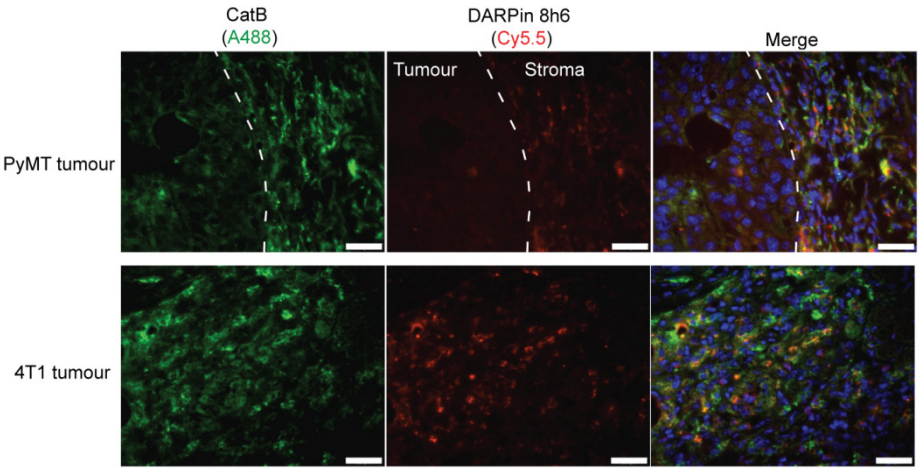

Figure S15 | Immunohistochemical analysis of cryopreserved tumours 3 h after intravenous administration of Cy5.5-labelled DARPin *8h6.* PyMT and 4T1 tumours from mice shown in main text Fig. 5 and Fig. 6 (3 h time-point after administration of Cy5.5-labelled DARPin *8h6*) were analysed. The tissue sections were stained for CatB (green; goat anti-mouse CatB polyclonal antibodies AF965, R&D at (1:500) and Alexa488-conjugated secondary anti-goat antibodies (1:1000, Thermo Fisher Scientific)) and for cell nuclei (DAPI, blue). Cy5.5 fluorescence of DARPin *8h6* is in red. Scale bar, 20 μm.

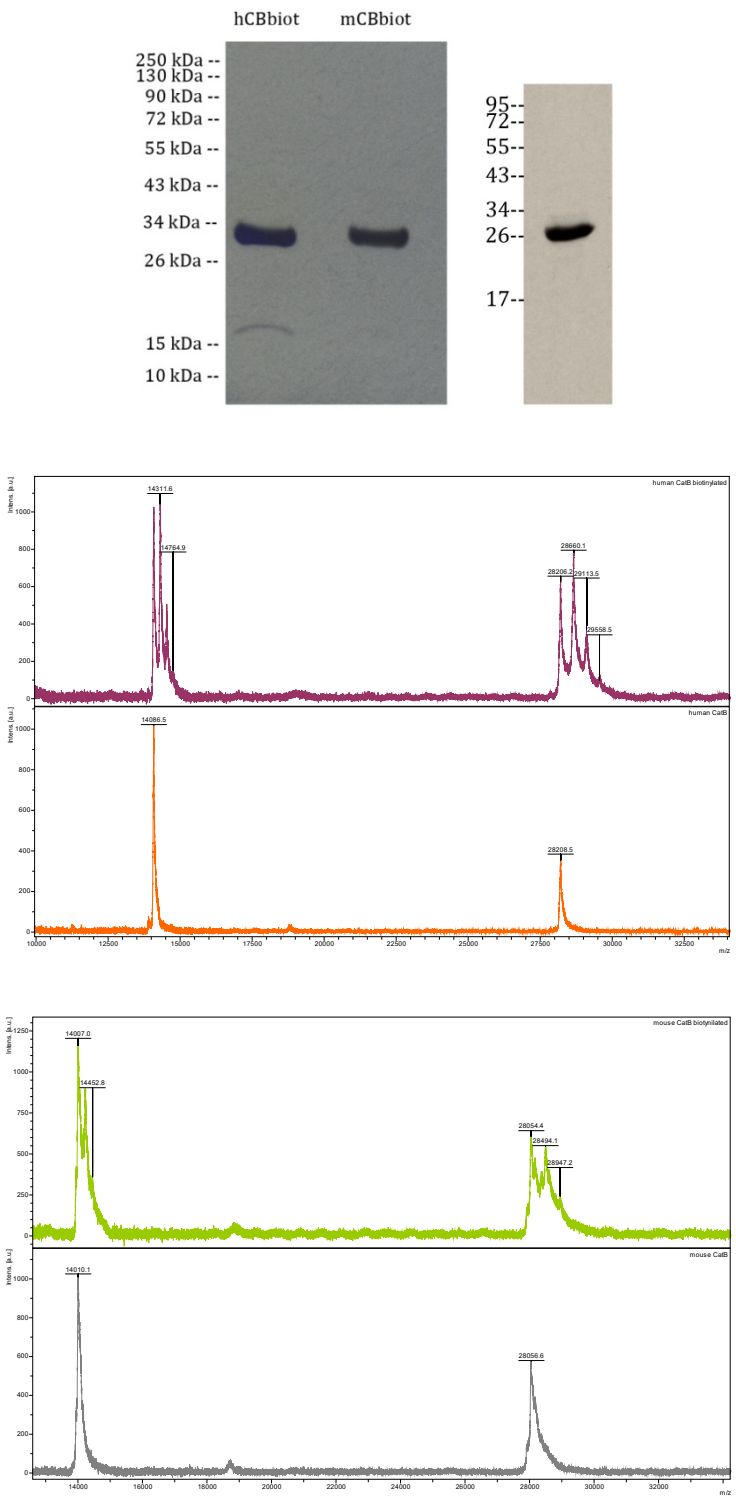

Figure S16 | Biotinylation of recombinant cathepsins. Upper panel: biotinylated cathepsins were separated using SDS-PAGE and blotted, and detection with streptavidin-HRP was performed. From left to right: human CatB, mouse CatB, human CatS. Lower

panel: MALDI-MS spectra of biotinylated and nonbiotinylated human CatB and mouse CatB. One to three biotin labels were detected in human CatB and one to two in mouse CatB.

SUPPLEMENTARY TABLES

Table S1 | Crystallization and crystal data collection

Crystal	DARPin 8h6	DARPin 81
Space group	$P2_12_12$	$P4_22_12$
Unit cell		
a, b, c (Å) **α,β,γ (deg)**	101.4, 201.5, 46.8 90, 90, 90	105.7, 105.7, 92.6 90, 90, 90
Complexes per asymmetric unit	2	1
Wavelength (Å)	0.91807	0.91807
Resolution range (Å)	46.8-2.76(2.93)	29.1-1.81(1.92)
No. of unique reflections	25129	48460
Completeness (%) (last shell)	0.98(93)	100(99.7)
CC ½	0.98(0.46)	1.0(0.96)
R-meas (last shell)	0.169(1.01)	0.066(0.067)
Average I/σ (last shell)	8.5(1.5)	26.7(4.0)
Refinement	**DARPin 8h6**	**DARPin 81**
PDB ID	5MBM	5MBL
Resolution range (Å)	46.8-2.76(2.81)	29.1-1.81(1.84)
No. of reflections in working set	25126(953)	48409(2370)
No. of reflections in test set	25126(953)	48409(2370)
Rvalue (%)	25.57(44.24)	16.97(25.66)
R-kick value (%)	28.05(46.73)	19.31(28.87)
RMSD deviation from ideal geometry **bond lengths (Å)** **bond angles (deg)**	 0.024 2.7	 0.021 2.08
Number of atoms in au **protein atoms** **water molecules** **$SO4^{2-}$**	 6356 143 /	 3174 541 1
Mean B value ($Å^2$)	63	31.8
Ramachandran plot statistics **favored** **allowed** **outliers**	 657 135 34	 410 12 3

SUPPLEMENTARY REFERENCES

1. Rozman J, Stojan J, Kuhelj R, Turk V, Turk B. Autocatalytic processing of recombinant human procathepsin B is a bimolecular process. FEBS letters. 1999; 459: 358-62.

2. Caglič D, Kosec G, Bojič L, Reinheckel T, Turk V, Turk B. Murine and human cathepsins B exhibit similar properties: possible implications for drug discovery. Biological Chemistry. 2009; 390: 175-9.

3. Mihelič M, Doberšek A, Gunčar G, Turk D. Inhibitory fragment from the p41 form of invariant chain can regulate activity of cysteine cathepsins in antigen presentation. Journal of Biological Chemistry. 2008; 283: 14453-60.

4. Bromme D, Nallaseth FS, Turk B. Production and activation of recombinant papain-like cysteine proteases. Methods. 2004; 32: 199-206.

5. Puzer L, Cotrin SS, Cezari MH, Hirata IY, Juliano MA, Stefe I, et al. Recombinant human cathepsin X is a carboxymonopeptidase only: a comparison with cathepsins B and L. Biological Chemistry. 2005; 386: 1191-5.

6. Seeger MA, Zbinden R, Flutsch A, Gutte PG, Engeler S, Roschitzki-Voser H, et al. Design, construction, and characterization of a second-generation DARP in library with reduced hydrophobicity. Protein Science. 2013; 22: 1239-57.

7. Zahnd C, Amstutz P, Pluckthun A. Ribosome display: selecting and evolving proteins in vitro that specifically bind to a target. Nature Methods. 2007; 4: 269-79.

8. Geertsma ER. FX cloning: a simple and robust high-throughput cloning method for protein expression. Methods in Molecular Biology. 2014; 1116: 153-64.

9. Studier FW. Protein production by auto-induction in high density shaking cultures. Protein Expression and Purification. 2005; 41: 207-34.

10. Binz HK, Stumpp MT, Forrer P, Amstutz P, Pluckthun A. Designing repeat proteins: well-expressed, soluble and stable proteins from combinatorial libraries of consensus ankyrin repeat proteins. Journal of Molecular Biology. 2003; 332: 489-503.

11. Martin-Killias P, Stefan N, Rothschild S, Pluckthun A, Zangemeister-Wittke U. A novel fusion toxin derived from an EpCAM-specific designed ankyrin repeat protein has potent antitumor activity. Clinical Cancer Research. 2011; 17: 100-10.

12. Kohl A, Binz HK, Forrer P, Stumpp MT, Plückthun A, Grütter MG. Designed to be stable: crystal structure of a consensus ankyrin repeat protein. Proceedings of the National Academy of Sciences. 2003; 100: 1700-5.

13. Szedlacsek SE, Ostafe V, Serban M, Vlad MO. A re-evaluation of the kinetic equations for hyperbolic tight-binding inhibition. Biochemical Journal. 1988; 254: 311-2.

14. Bravman T, Bronner V, Lavie K, Notcovich A, Papalia GA, Myszka DG. Exploring "one-shot" kinetics and small molecule analysis using the ProteOn XPR36 array biosensor. Analytical Biochemistry. 2006; 358: 281-8.